# Germanium nanowire microbolometer



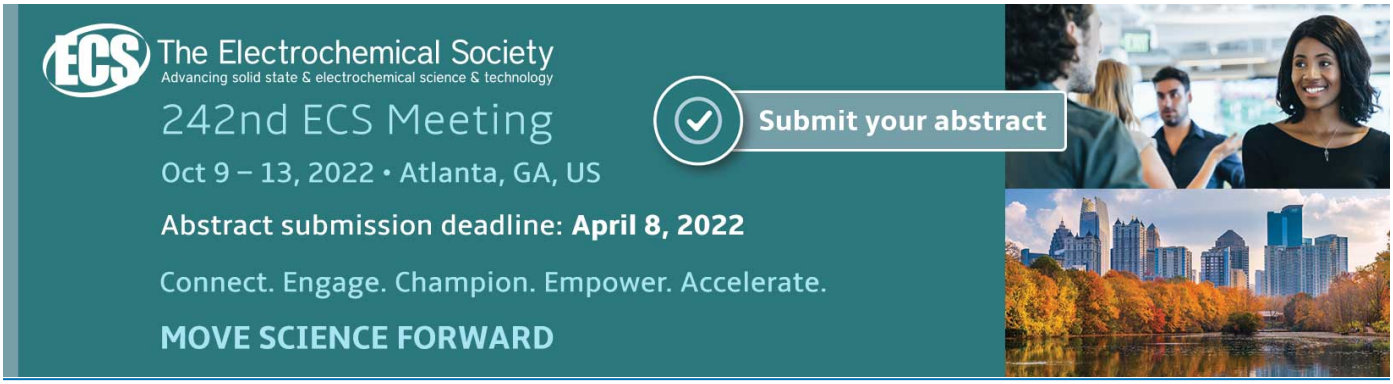

OPEN ACCESS
IOP Publishing
Nanotechnology

Nanotechnology **33** (2022) 245201 (6pp)
https://doi.org/10.1088/1361-6528/ac5aec

# Germanium nanowire microbolometer

**M G Bartmann[1], M Sistani[1], N Luhmann[2], S Schmid[2], E Bertagnolli[1], A Lugstein[1] and J Smoliner[1]**

[1] Technische Universität Wien, Institute of Solid State Electronics, Vienna, Austria
[2] Technische Universität Wien, Institute of Sensor and Actuator Systems, Vienna, Austria

E-mail: alois.lugstein@tuwien.ac.at

Received 5 January 2022, revised 17 February 2022
Accepted for publication 4 March 2022
Published 23 March 2022

**Abstract**

Near-infrared detection is widely used for nondestructive and non-contact inspections in various areas, including thermography, environmental and chemical analysis as well as food and medical diagnoses. Common room temperature bolometer-type infrared sensors are based on architectures in the $\mu$m range, limiting miniaturization for future highly integrated 'More than Moore' concepts. In this work, we present a first principle study on a highly scalable and CMOS compatible bolometer-type detector utilizing Ge nanowires as the thermal sensitive element. For this approach, we implemented the Ge nanowires on top of a low thermal conducting and highly absorptive membrane as a near infrared (IR) sensor element. We adopted a freestanding membrane coated with an impedance matched platinum absorber demonstrating wavelength independent absorptivity of 50% in the near to mid IR regime. The electrical characteristics of the device were measured depending on temperature and biasing conditions. A strong dependence of the resistance on the temperature was shown with a maximum temperature coefficient of resistance of $-0.07\ K^{-1}$ at $T = 100$ K. Heat transport simulations using COMSOL were used to optimize the responsivity and temporal response, which are in good agreement with the experimental results. Further, lock-in measurements were used to benchmark the bolometer device at room temperature with respect to detectivity and noise equivalent power. Finally, we demonstrated that by operating the bolometer with a network of parallel nanowires, both detectivity and noise equivalent power can be effectively improved.

Supplementary material for this article is available online

Keywords: bolometer, germanium, nanowire

(Some figures may appear in colour only in the online journal)

The ever increasing demand for more compact and mobile sensor systems intensifies the need for highly miniaturized device architectures [1]. The same trend has been observed before in the continuous downscaling of modern integrated circuits (ICs), following Moore's Law [2]. Today, transistors have evolved to quasi 1D structures, which are also referred to as nanowires (NWs) enabling superior electrostatic control of the transistor channel and thus scaling of ICs to the 5 nm technology node and below [3–5]. In this context, the development of a NW based detector presents itself as an obvious consequence, since this would allow the implementation of an additional functionality level into CMOS-based technologies, enabling cost optimization and value-added system solutions [6].

Among the manifold techniques for the detection of electromagnetic waves, bolometric sensing represents a highly versatile approach [7, 8]. It offers the ability of detecting photons over a large spectral bandwidth and ideally also at ambient temperatures [8]. Thus, in the IR bolometers are widely used. This spectral band ranging from 700 nm to 1 mm plays an important role in manifold modern scientific and commercial technologies including thermography, [7, 9, 10] optical communication, [11, 12] observation of astronomical phenomena [7, 13, 14] and foremost chemical sensing of molecules. [1, 15].

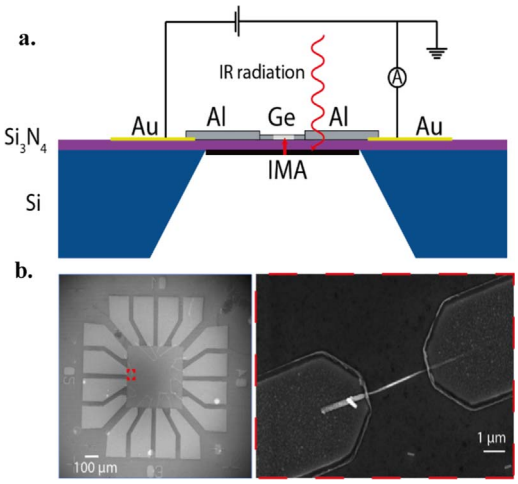


**Figure 1.** (a) Schematic illustration of the Ge NW microbolometer. The $Al_2O_3$ passivated Ge NW atop of a freestanding $Si_3N_4$ membrane is electrically contacted by monolithic Al leads. The backside of the membrane is conformal coated with a thin Pt layer acting as an IMA for the incident IR radiation. The resulting increase of the membrane temperature due to IR exposure leads to a conductivity enhancement in the NW which is detected electrically. (b) SEM image of a fully featured NW bolometer. The NWs atop of the membrane are electrically contacted via monolithic Al leads to macroscopic Au pads at the surrounding of the membrane. The right image shows a magnified view of an individual Ge NW with the monolithic Al contacts.

The core parts of a bolometer are a broadband absorber and a detector element whose resistance is strongly temperature-dependent [16]. For the fabricated bolometer device the radiation is absorbed by an impedance matched absorbing (IMA) metal layer (see supplementary material available online at stacks.iop.org/NANO/33/245201/mmedia). The heat generated in the IMA is transferred to the sensing element and the resulting change in conductivity is measured by an electrical read-out circle. In this work, we present a Ge NW bolometer on an $Si_3N_4$ membrane coated by an IMA as absorbing layer. In the past, bulk Ge has often been used for bolometers as it can be produced in high purity and due to its physicochemical properties, particularly the high temperature dependent resistance [17–19]. With regard to the embedding of detectors in ICs already mentioned above, it is also important here to mentioned that, Ge can be monolithically integrated in silicon platform technology [20–22].

Here, we present a CMOS compatible, highly integrated microbolometer device based on vapor–liquid–solid [23] grown Ge NWs as the temperature sensing element on a $Si_3N_4$ membrane with a Pt based IMA for the IR regime [24]. Figure 1(a) shows the schematic of the fully featured device. The Ge NW (details of NW growth can be found in the supporting information) with a diameter of 15 nm is deposited on a 50 nm thick $Si_3N_4$ membrane with the IMA on the back-side consisting of a 5 nm thick Pt layer. Reliable electrical contacts are achieved by a thermal induced exchange reaction with Al pads, [25] further connected to macroscopic Au pads. The Ge NWs are coated with a 20 nm thick $Al_2O_3$ passivation layer (not shown in the schematic) to enhance the conductivity of the channel and reduce the influence of acceptor-like surface

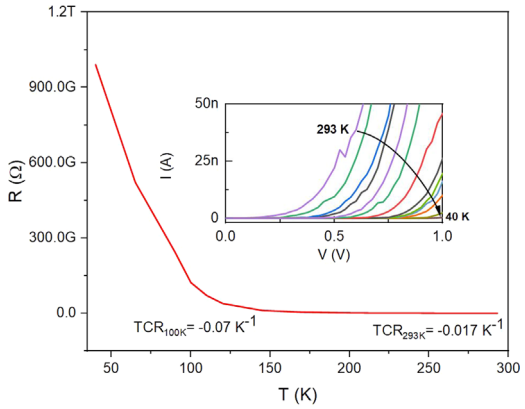


**Figure 2.** Temperature dependent resistance of a 15 nm thick and 730 nm long Ge segment passivated with 20 nm $Al_2O_3$. The TCR values determined at 293 K and 100 K are inserted. The inset depicts the $I/V$ characteristic at various temperatures.

trap states, which are well known for dominating the electrical behavior of bare Ge NWs [26, 27].

Figure 1(b) shows a SEM image of the fully featured test device consisting of several contacted NWs atop of the suspended $Si_3N_4$ membrane with an area of (800 × 800) $\mu m^2$. In the actual device the area of the Al leads contacting the Al–Ge–Al NW heterostructure is small (<1%) compared to the size of the IR absorbing membrane. Thus, the effect of optical coupling via the Al leads may be considered to be negligible.

Figure 2(b) further shows a magnified view of an individual Ge NW (red marked square in figure 1(b)) with the Ge segment contacted by single crystalline Al leads. As already mentioned above, the Al–Ge–Al heterostructure was formed by a thermal induced exchange reaction, performed at the very end of the processing. For this purpose, the device was heated via rapid thermal annealing to 623 K. This temperature is maintained for a certain period of time in order to adjust the Ge segment length and to achieve reliable electrical contacts. [25, 26, 28].

To generate a significant electrical signal change upon temperature increase, the detector element of the bolometer is required to exhibit a large temperature coefficient of resistance (TCR) which is defined as follows:

$$TCR = \frac{1}{R_0} * \frac{dR}{dT} \tag{1}$$

with $R_0$ denoting the resistance at the operational temperature and $\frac{dR}{dT}$ the resistance change per Kelvin [8] as a semiconductor, Ge exhibits a negative TCR [16] of about −0.01 to −0.06 $K^{-1}$, depending on doping and crystallinity. [17–19] figure 2 shows the resistance as a function of temperature from a typical Al–Ge–Al heterostructure comprising a nominally intrinsic, 15 nm thick and 730 nm long Ge NW segment, passivated by an about 20 nm thick $Al_2O_3$ layer. The resistance was extracted from the linear region in the respective $I/V$ characteristics shown in the inset.

As the device shows a nonlinear $I/V$-behavior, the $R(T)$ data was acquired recording $I/V$ curves in the temperature range between $T = 40$ K and 293 K and extracting the

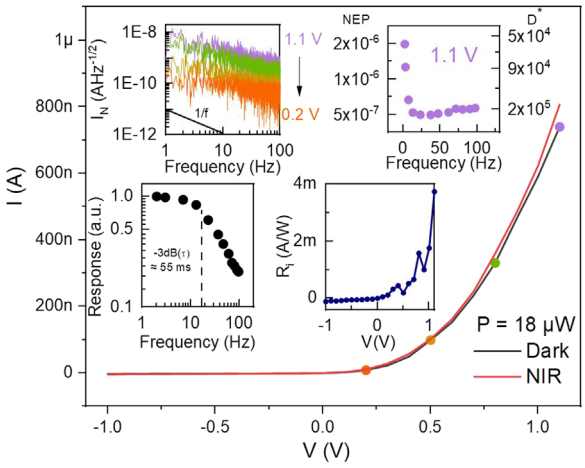


**Figure 3.** $I/V$ characteristic of a Ge NW in the dark (grey) and under illumination with a tungsten globar (red). The bottom right inset illustrates the extracted current responsivity with a peak value of 3.7 mA W$^{-1}$ at 1.1 V. The bottom left inset shows the measured frequency dependent response yielding a thermal time constant of ≈55 ms. The top left inset depicts the measured current noise along the $I/V$ characteristic at the corresponding colored points in the main plot. The top right inset shows the frequency dependent NEP and $D^*$ at the point of the highest $R_i$. The lowest NEP value occurs at 37 Hz with 4.9*10$^{-7}$ WHz$^{-1/2}$ which corresponds to a $D^*$ of 1.6*10 $^5$ cmHz$^{1/2}$ W$^{-1}$.

resistance in the linear part of the $I/V$ characteristic by linear fitting of the measured data. Starting from 40 K, upon increasing temperature, the thermal generation of charge carriers result in a strong decrease in resistance. The highest TCR was observed at 100 K with a value of about −0.07 K$^{-1}$.

Prior to the integration of the Al–Ge–Al heterostructure in the bolometer device, heat transport simulations have been performed to determine the optimal membrane size, which essentially determines the overall temperature rise and the temporal behavior of the bolometer. For this purpose, the structure was evaluated using COMSOL Multiphysics® (see supplementary material).

For such an optimized membrane with (800 × 800) $\mu$m$^2$ a temperature increase of 4 K can be expected for the actual IR excitation power of $P = 18$ $\mu$W. With regard to the temporal behavior of the bolometer, a thermal time constant $\tau$, which is defined as the −3 dB roll-off from the dc responsivity [29] was calculated with ≈35 ms.

To characterize the current responsivity $R_i$ of the microbolometer, the $I/V$ characteristic of an individual NW on top of the membrane was measured under IR illumination. Therefore, the sample was placed in a cryostat (Oxford® OptistatDry) with a $CaF_2$ window and electrically connected to a Semiconductor Analyzer (Keithley 4200 SCS). Homogeneous illumination was achieved using the Tungsten IR globar of a FTIR (Bruker® Vertex 70) focused on the microbolometer through a low pass filter and the above mentioned IR transparent $CaF_2$ window. Figure 3 depicts the $I/V$ characteristic with (red) and without IR illumination (black). Notably, all measurements were performed in voltage biasing mode with a current compliance of 1 $\mu$A [30].

This has two purposes: Firstly, it prevents the avalanche like increase of the current, which would most probably damage the device. Secondly, it avoids self-heating via Joule-Heating. This limit however is a rigorous safety measure, since previous spatial thermal analysis of our NWs showed, that the onset of Joule heating for a Ge segment of 168 nm is in the order of $P = 25$ $\mu$W dissipated Joule heating power ($P = I^* V$). [30].

What is immediately noticeable is the rectifying behavior of the device which is in contrast to previous studies of $Al_2O_3$ passivated Ge NWs on oxidized Si wafers [25]. In contrast to these, the bolometer device has a homogeneous Pt film on the back of the membrane acting as the IMA. This large area metal layer is separated from the Ge NW by only a 50 nm thick $Si_3N_4$ dielectric layer and therefore acts as a very effective floating gate.

The asymmetry in the $I/V$ characteristics is commonly misinterpreted as an evidence of non-ohmic metal-semiconductor interface. However, we argue that the asymmetry observed in the $I/V$ response is indicative of the channel potential and the surface potential. This effect is related to the NW geometry and is a direct consequence of the channel pinch-off, which for p-channel devices can only occur for negative bias voltages [31]. However, upon illumination with an overall power of 18 $\mu$W, the current increases both for negative and positive applied bias voltage. The extracted corresponding responsivity is displayed in the bottom right inset with the highest $R_i$ at 1.1 V with 3.7 mA W$^{-1}$. As can be seen very clearly, a further increase in the bias voltage should increase the $R_i$ even further. However, it must be considered that this would lead to a self-heating of the bolometer due to Joule heating effects, [30] which would then have to be taken into account accordingly in the evaluation of the performance. For the actual device, the voltage bias operation of a Ge NW exhibiting a negative TCR, would result in a positive electrothermal feedback increasing both responsivity and time constant [32]. Although, as the thermal time constant of the device is mainly dominated by the membrane an altered time constant appears unlikely. From the data in the linear region and using the TCR of −0.017 K$^{-1}$ determined at room temperature, we calculated a temperature increase of about 4.4 K, which is in good agreement with the simulated temperature increase of ≈4 K.

To determine key performance parameters for a bolometer, namely the Noise Equivalent Power (NEP), the thermal time constant $\tau$ and the current noise spectral density ($I_n$), lock-in (Zuerich Instruments® MFLI 500 kHz/5 MHz) measurements were performed with a chopper modulating the intensity of the IR beam. The NEP is defined in the case of current sensing as the fraction of the current noise spectral density and the responsivity, [16]

$$NEP = \frac{I_n}{R_i}. \tag{2}$$

First we have investigated the frequency dependent response by observing the current response at different chopper frequency. This is depicted in the bottom left inset of figure 3. For small chopping frequencies up to 7 Hz the response of the device remains almost constant. In this region, the device can reach thermal equilibrium resulting in a constant response. At higher frequencies, the response decreases and above 41 Hz it drops according a $1/f$ behavior. The extracted time constant is $\tau \approx 55$ ms, which is higher than the simulated value of $\tau \approx 35$ ms. This is most likely due to the fact that we realized more than one NW device on the membrane to investigate also NW arrays as discussed below and that the sample has to be glued to a sample holder. Thus, this increase of the thermal mass may increase the thermal time constant. However, in accordance with previous works by Piller *et al* [33], our simulations (see supplementary material) have shown that $\tau$ can be effectively decreased using smaller membranes even if at the cost of responsivity.

Finally, the current noise spectral density shown in the top left inset was determined at the four points marked in the $I/V$ characteristic of the main plot in figure 3. The overall noise in the observed range decrease by about 1.5 order of magnitude when the bias is reduced from 1.1 V to 0.2 V. Although a smaller bias voltage and thus current flow inside the channel results in a noise reduction, we found that the NEP in the investigated regime is mainly dominated by $R_i$. In consequence, the lowest NEP was observed at the highest investigated bias of 1.1 V with $4.9^{*}10^{-7}$ W $\mathrm{Hz}^{-1/2}$ at a frequency of 37 Hz (top right inset in figure 3).

The most meaningful figure of merit for bolometers that also includes the active absorbing area of the detector and the signal bandwidth is the normalized detectivity ($D^{*}$):

$$D^{*} = \frac{\sqrt{A_d \Delta f}}{NEP}. \tag{3}$$

This is represented by the right axis in the top right inset in figure 3 and characterizes the detector output signal-to-noise ratio at 1 W of input IR radiation normalized to a detector with a unit active area and a 1 Hz bandwidth. With an active area of $(800 \times 800)$ $\mu\mathrm{m}^2$, this results in a $D^{*}$ of $1.6^{*}10^{5}$ $\mathrm{cmHz}^{1/2}$ $\mathrm{W}^{-1}$ at 37 Hz (top right inset in figure 3).

To improve the performance of the bolometer device in terms of NEP and further $D^{*}$, two possible approaches can be conceived (equation 2): increasing $R_i$ or decreasing $I_n$. As already mentioned above, the responsivity $R_i$ of the bolometer could be increased very effectively by increasing the bias voltage (see bottom right inset in figure 3). However, for a future operation of a Ge NW microbolometer at higher current levels one has to consider several additional aspects such as the above mentioned Joule heating in the Ge NW, [30] inducing a positive electrothermal feedback which further impacts the responsivity and time constant [32] as well as the overall increased noise [34].

With regard to a targeted reduction of noise, it is important to note that in the case of NWs, this is mainly determined by the large surface to volume ratio. It is well known that electrical devices based on NWs show a significant increase in electrical noise when compared to bulk material [35]. This has been observed in a variety of materials including Ge [36], Si [37], III–V [38] as well as metal oxide NWs [39], with the excess noise mainly attributed to surface charge trapping and de-trapping as well as surface scattering related noise [36, 38, 39]. In consequence, the low frequency noise in Ge NWs is dominated by random telegraph signals and $1/f$ noise [36]. Other noise sources such as shot and contact noise can be neglected at low current levels [40] and the excellent quality [36, 41] of the monolithic Al–Ge contacts respectively.

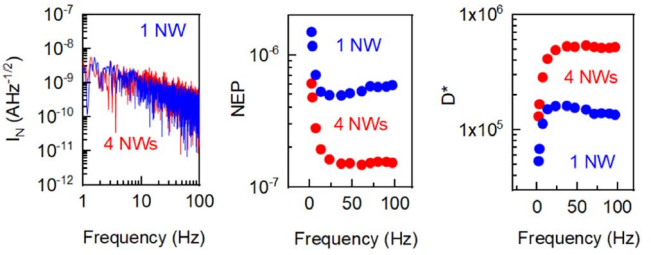


**Figure 4.** (a) The measured frequency dependent current noise for 4 NWs compared to the current noise of an individual NW. (b) A comparison between the NEP of 4 NWs and a single NW. (c) A comparison between the $D^{*}$ of 4 NWs and a single NW.

Therefore, an approach to increase responsivity via increasing the current output [42], while simultaneously increasing noise less than linear [40], would be to use an ensemble of parallel NWs as detector element.

Having only a minor impact on the overall current noise, the parallelization has a positive impact on the Johnson Noise which only depends on the resistance of the circuit [16]. Further the $1/f$ noise originating from the above described trapping events [36] should be uncorrelated and therefore increase less than linear due to statistical averaging [40]. In addition an increased current output should raise the $R_i$. To determine the performance for a network of NWs we connected four Ge NWs across the membrane area in a parallel manner.

Figure 4 shows the comparison of $I_N$ (a), NEP (b) and $D^{*}$ (c) for a bolometer device with one or four parallel NWs as temperature sensing element. For the measurements with 4 parallel nanowires, components were selected which were far apart from each other and having minimal length of the bulk Al contacts to the Al–Ge–Al heterostructures to minimize uncontrolled heat dissipation through the metal contacts.

The corresponding $I_N$ of the device with four NWs is depict in figure 4(a) (red curve) alongside with the previously determined $I_n$ of a device with only one NW (blue curve). Here, we measured a largely unchanged current noise for four NWs at 530 nA in the observed bandwidth when comparing to the noise levels for a single NW (figure 4(a)). This constant current noise for the increased number of NWs can be dedicated to the fact that the above described main noise source ($1/f$-noise) of NWs is uncorrelated. In consequence, by using a parallel array of NWs this will raise the intrinsic noise level less than linear due to statistical averaging [40]. For the small increase from one to four NWs we could not measure a

significant elevation of the noise level. In contrast to the current noise levels a noticeable increase of $R_i$ from 3.8 mA $W^{-1}$ to 5.2 mA $W^{-1}$ was observed due to an increase of the transconductance of parallel NW networks compared to single NWs. [42]. As a combined effect the measured NEP and $D^*$ of the NW network are $1.7^*10^{-7}$ $WHz^{-1/2}$ and $5.4^*10^5$ $cmHz^{1/2}$ $W^{-1}$ respectively. This corresponds to an improvement by a factor of 2.8 and 3.3 respectively. Comparing the observed NEP and $D^*$ to a selection of previously reported bolometer devices in the literature (see supplementary material), the presented microbolometer still requires further improvement in terms of NEP/$D^*$ by 2 orders of magnitude to reach a competitive sensitivity. A further increase in the number of NWs connected in parallel should lead to a corresponding improvement in performance. However, to generate a net improvement in NEP and $D^*$, the current noise has to be rather constant or at least show a smaller increase than the corresponding $R_i$. For future investigations and applications, it is therefore necessary to develop a top-down process that allows the production of thousands of Ge NWs on the membrane. In this way, the doping and passivation of the NWs can also be improved with the aim of increasing the TCR and decreasing $I_n$ respectively, leading to a smaller NEP. Further, an improved thermal isolation to the support structure can prevent temperature dissipation and thus lead to increased responsiveness. This should result in a smaller NEP, however most likely at the cost of an increased $\tau$. Finally, improved thermal isolation of the membrane chip to the support structure can prevent temperature dissipation and thus lead to increased responsiveness. This should result in a smaller NEP, however again most likely at the cost of an increased $\tau$.

In conclusion, we demonstrated a CMOS compatible Ge NW based microbolometer, which paves the way for future highly integrated 'More than Moore' concepts. We showed that a membrane based architecture can be effectively tuned by altering the membrane area which influences both detector speed and temperature increase in the NW. Furthermore, it was shown that the performance of the bolometer can be improved not only by an optimized component architecture but also by the use of many NWs connected in parallel as temperature-sensitive elements.

## Acknowledgments

The authors gratefully acknowledge financial support by the Austrian Science Fund (FWF): Project No. P29729-N27. This work has received funding from the European Union's Horizon 2020 research and innovation program (Grant Agreement-716087-PLASMECS). The authors further thank the Center for Micro- and Nanostructures for providing the cleanroom facilities.

## Data availability statement

The data that support the findings of this study are available upon reasonable request from the authors.

## Author's contributions

M G B wrote the manuscript.

M G B and M S conducted the electrical and optical measurements.

M G B , M S and N L performed the fabrication of the samples.

S S and N L provided the IMA coated $Si_3N_4$ membranes as well as theoretical expertize.

A L, J S and E B conceived the project and contributed essentially to the experimental design.

## ORCID iDs

M G Bartmann https://orcid.org/0000-0002-9556-1550
M Sistani https://orcid.org/0000-0001-5730-234X
A Lugstein https://orcid.org/0000-0001-5693-4775

## References

[1] Schwarz B, Reininger P, Ristanić D, Detz H, Andrews A M, Schrenk W and Strasser G 2014 Monolithically integrated mid-infrared lab-on-a-chip using plasmonics and quantum cascade structures *Nat. Commun.* **5** 4085
[2] Ahmed K and Schuegraf K 2011 Transistor wars *IEEE Spectr.* **48** 50–66
[3] Loubet N *et al* 2017 Stacked nanosheet gate-all-around transistor to enable scaling beyond FinFET *2017 Symp. on VLSI Technology* vol 5 (IEEE) pp T230–1
[4] Lu W, Xie P and Lieber C M 2008 Nanowire transistor performance limits and applications *IEEE Trans. Electron Devices* **55** 2859–76
[5] Hiramoto T 2019 Five nanometre CMOS technology *Nat. Electron.* **2** 557–8
[6] Cavin R K, Lugli P and Zhirnov V V 2012 Science and engineering beyond moore's law *Proc. IEEE* **100** 1720–49
[7] Blaikie A, Miller D and Alemán B J 2018 A fast, sensitive, room-temperature graphene nanomechanical bolometer *Nat. Commun.* **10** 4726
[8] Sassi U *et al* 2017 Graphene-based mid-infrared room-temperature pyroelectric bolometers with ultrahigh temperature coefficient of resistance *Nat. Commun.* **8** 14311
[9] Landmann M, Heist S, Dietrich P, Lutzke P, Gebhart I, Templin J, Kühmstedt P, Tünnermann A and Notni G 2019 High-speed 3D thermography *Opt. Lasers Eng.* **121** 448–55
[10] Ciampa F, Mahmoodi P, Pinto F and Meo M 2018 Recent Advances in Active Infrared Thermography for Non-Destructive Testing of Aerospace Components *Sensors* **18** 609
[11] Fermann M E and Hartl I 2013 Ultrafast fibre lasers *Nat. Photon.* **7** 868–74
[12] John S 2009 *Optical Fiber Communications: Principles and Practice, 3rd Edition* (Englewood Cliffs, NJ: Prentice-Hall)

[13] Graur O, Maguire K, Ryan R, Nicholl M, Avelino A, Riess A G, Shingles L, Seitenzahl I R and Fisher R 2020 A year-long plateau in the late-time near-infrared light curves of type Ia supernovae *Nat. Astron.* **4** 188–95
[14] Richards P L and McCreight C R 2005 Infrared detectors for astrophysics *Phys. Today* **58** 41–7
[15] Réhault J, Borrego-Varillas R, Oriana A, Manzoni C, Hauri C P, Helbing J and Cerullo G 2017 Fourier transform spectroscopy in the vibrational fingerprint region with a birefringent interferometer *Opt. Express* **25** 4403
[16] Rogalski A 2010 *Infrared Detector Characterization Infrared Detectors, Second Edition* (Boca Raton, FL: CRC Press) 23–34
[17] Enukova T A, Ivanova N L, Kulikov Y V, Malyarov V G and Khrebtov I A 1997 Amorphous silicon and germanium films for uncooled microbolometers *Tech. Phys. Lett.* **23** 504–6
[18] Bullis W M, Brewer F H, Kolstad C D and Swartzendruber L J 1968 Temperature coefficient of resistivity of silicon and germanium near room temperature *Solid State Electron.* **11** 639–46
[19] Torres A 2003 Uncooled micro-bolometer based on amorphous germanium film *J. Non-Cryst. Solids* **329** 179–83
[20] Chen C, Li C, Huang S, Zheng Y, Lai H and Chen S 2012 Epitaxial growth of germanium on silicon for light emitters *Int. J. Photoenergy* **2012** 1–8
[21] Ayala J, Bell J, Nummy K, Guan F and Hu S 2019 Integrating a high performance Germanium photodiode into a CMOS compatible flow for a full monolithic silicon photonics solution *2019 30th Annual SEMI Advanced Semiconductor Manufacturing Conf. (ASMC) (IEEE)* pp 1–4
[23] Wagner R S and Ellis W C 1964 Vapor–liquid–solid mechanism of single crystal growth *Appl. Phys. Lett.* **4** 89–90
[24] Luhmann N, Høj D, Piller M, Kähler H, Chien M-H, West R G, Andersen U L and Schmid S 2019 Ultrathin 2 nm gold as ideal impedance-matched absorber for infrared light *Nat. Commun.* **11** 2161
[25] Kral S, Zeiner C, Stöger-Pollach M, Bertagnolli E, Den Hertog M I, Lopez-Haro M, Robin E, El Hajraoui K and Lugstein A 2015 Abrupt schottky junctions in al/ge nanowire heterostructures *Nano Lett.* **15** 4783–7
[26] Sistani M, Staudinger P, Greil J, Holzbauer M, Detz H, Bertagnolli E and Lugstein A 2017 Room-temperature quantum ballistic transport in monolithic ultrascaled Al–Ge–Al nanowire heterostructures *Nano Lett.* **17** 4556–61
[27] Sistani M, Staudinger P and Lugstein A 2020 Polarity control in ge nanowires by electronic surface doping *J. Phys. Chem. C* **124** 19858–63
[28] El Hajraoui K, Luong M A, Robin E, Brunbauer F, Zeiner C, Lugstein A, Gentile P, Rouvière J-L and Den Hertog M 2019 *In situ* transmission electron microscopy analysis of aluminum–germanium nanowire solid-state reaction *Nano Lett.* **19** 2897–904
[29] Anon 2015 *Detectors: Figures of Merit Encyclopedia of Optical and Photonic Engineering, Second Edition* (Boca Raton, FL: CRC Press) 1–9
[30] Gächter N, Könemann F, Sistani M, Bartmann M G, Sousa M, Staudinger P, Lugstein A and Gotsmann B 2020 Spatially resolved thermoelectric effects in operando semiconductor–metal nanowire heterostructures *Nanoscale* **12** 20590–7
[31] Kumar Bhaskar U, Pardoen T, Passi V and Raskin J-P 2013 Surface states and conductivity of silicon nano-wires *J. Appl. Phys.* **113** 134502
[32] Wood R A 1997 Chapter 3 monolithic silicon microbolometer arrays *Semicond. Semimet.* **47** 43–121d
[33] Piller M, Sadeghi P, West R G, Luhmann N, Martini P, Hansen O and Schmid S 2020 Thermal radiation dominated heat transfer in nanomechanical silicon nitride drum resonators *Appl. Phys. Lett.* **117** 034101
[34] Tikhonov E S, Shovkun D V, Ercolani D, Rossella F, Rocci M, Sorba L, Roddaro S and Khrapai V S 2016 Local noise in a diffusive conductor *Sci. Rep.* **6** 30621
[35] Bid A, Bora A and Raychaudhuri A K 2006 $1/f$ noise in nanowires *Nanotechnology* **17** 152–6
[36] Pogany D, Zeiner C, Bychikhin S, Burchhart T, Lugstein A and Vandamme L K J 2011 RTS and $1/f$ noise in Ge nanowire transistors *2011 21st Int. Conf. on Noise and Fluctuations (IEEE)* pp 368–371
[37] Reza S, Bosman G, Islam M S, Kamins T I, Sharma S and Williams R S 2006 Noise in silicon nanowires *IEEE Trans. Nanotechnol.* **5** 523–9
[38] Persson K-M, Lind E, Dey A W, Thelander C, Sjoland H and Wernersson L-E 2010 Low-frequency noise in vertical InAs nanowire FETs *IEEE Electron Device Lett.* **31** 428–30
[39] Ju S, Chen P, Zhou C, Ha Y G, Facchetti A, Marks T J, Kim S K, Mohammadi S and Janes D B 2008 $1f$ noise of $SnO_2$ nanowire transistors *Appl. Phys. Lett.* **92** 2–5
[40] Pregl S, Baraban L, Sessi V, Mikolajick T, Weber W M and Cuniberti G 2018 Signal and noise of Schottky-junction parallel silicon nanowire transducers for biochemical sensing *IEEE Sens. J.* **18** 967–75
[41] Delaforce J *et al* 2021 Al–Ge–Al nanowire heterostructure: from single-hole quantum dot to Josephson effect *Adv. Mater.* **33** 2101989
[42] Pregl S, Weber W M, Nozaki D, Kunstmann J, Baraban L, Opitz J, Mikolajick T and Cuniberti G 2013 Parallel arrays of Schottky barrier nanowire field effect transistors: nanoscopic effects for macroscopic current output *Nano Res.* **6** 381–8